ACS Catalysis

Research Article

pubs.acs.org/acscatalysis

Understanding the Role of Oxygen Vacancies in the Water Gas Shift Reaction on Ceria-Supported Platinum Catalysts

Julia Vecchietti,[†] Adrian Bonivardi,[†] Wenqian Xu,[‡] Dario Stacchiola,[‡] Juan J. Delgado,[§] Monica Calatayud,[∥,⊥] and Sebastián E. Collins*[,†]

[†]Instituto de Desarrollo Tecnológico para la Industria Química (INTEC) UNL-CONICET, Güemes 3450, 3000 Santa Fe, Argentina

[‡]Department of Chemistry, Brookhaven National Laboratory, Upton, New York 11973, United States

[§]Departamento de de Ciencia de los Materiales e Ingeniería Metalúrgica y Química Inorgánica, Facultad de Ciencias, Universidad de Cádiz, Campus Río San Pedro, 11510 Puerto Real, Cádiz, Spain

[∥]Institut Universitaire de France, Laboratoire de Chimie Théorique, Université Piere et Marie Curie and CNRS, UMR 7616, F-75005 Paris, France

Supporting Information

ABSTRACT: Reducible oxides have been shown to greatly improve the activity of water gas shift (WGS) catalysts. The precise mechanism for this effect is a matter of intense debate, but the dissociation of water is generally considered to be the key step in the reaction. We present here a study of the water activation on oxygen vacancies at the support as part of the mechanism of the WGS reaction on Pt supported on pure and gallium-doped ceria. Doping the ceria with gallium allows tuning the vacancies in the support while maintaining constant the metal dispersion. An inverse relationship was found between the catalytic activity to WGS and the amount of oxygen vacancies. In situ time-resolved X-ray diffraction, mass spectrometry, and diffuse reflectance infrared spectroscopy (DRIFT) showed that the oxygen vacancy filling by water is always fast in either Pt/CeO_2 or Pt/CeGa. DFT calculation provides molecular insights to understand the pathway of water reaction with vacancies at the metal−oxide interface sites. Our results suggest that the activation of the water molecule in the WGS mechanism is not the rate-limiting step in these systems. Concentration-modulation spectroscopy in DRIFT mode under WGS reaction conditions allows the selective detection of key reaction intermediates, a monodentate formate (HCOO) and carboxylate ($CO_2^{\delta-}$) species, which suggests the prevalence of a carboxyl (HOCO) mechanism activated at the oxide−metal interface of the catalyst.

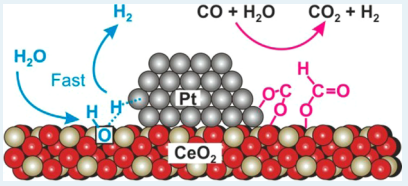

KEYWORDS: *water gas shift, platinum, ceria, reaction mechanism, in situ spectroscopies, DRIFT, time-resolved X-ray diffraction*

1. INTRODUCTION

The need for high-purity hydrogen with <50 ppm of CO to feed polymer electrolyte membrane fuel cells has prompted the investigation of active catalysts for the low-temperature water gas shift reaction (LT-WGS).[1] The WGS reaction is equilibrium-limited and moderately exothermic ($CO + H_2O \rightarrow H_2 + CO_2$; $\Delta H^0 = -41$ kJ/mol). Therefore, to achieve very low CO concentration levels, catalysts active at temperatures as low as 423 K are needed.[2] Fundamental understanding of the WGS reaction mechanism at the molecular level is certainly an important tool toward the design of suitably catalytic materials to accomplish such requirements. Metal-supported (gold and platinum) ceria-based catalysts are among the best candidates to meet these demands.[2]

Two main reaction mechanisms have been proposed in the literature: (i) the redox and (ii) the associative mechanisms. Both mechanisms proposed are bifunctional, that is, they involve the metal particles and the oxidic support as active sites. In the redox mechanism, CO adsorbed on metal sites reacts with an oxygen atom from the support to produce CO_2, and subsequently, water replenishes the generated oxygen vacancy.[3−6] In the associative mechanism, different pathways involving formate (HCOO),[7−11] carbonate (CO_3),[12,13] or carboxyl (HOCO)/carboxylate ($CO_2^{\delta-}$)[14−17] species as key intermediates have been proposed. Recently, Burch and Meunier[18] thoroughly analyzed the evidence for and against the formate associative mechanism, concluding that there is no substantial data that unambiguously prove any of the WGS mechanisms proposed for the highly active catalysts. The associative carboxyl mechanism was first theoretically proposed[15,16] and has now been experimentally shown on model catalysts.[17] Nevertheless, both redox and associative mechanisms involve a water dissociation step. Although this reaction stage has received less attention in the investigations of the WGS mechanism, it has been reported as energetically important and, in some cases, as the rate-determining step of the WGS reaction.[14,19−21] Thus, the role of the oxygen vacancies on reducible supports has been highlighted, particularly with regard to the activity of ceria-based catalysts. Rodriguez et al. found that the most difficult step in the WGS

Received: March 12, 2014
Revised: May 15, 2014

   dx.doi.org/10.1021/cs500323u | ACS Catal. 2014, 4, 2088−2096

on model Au_{29} and Cu_{29} clusters was water dissociation and proposed that on the supported ones, the reduced $CeO_2(111)$ surface facilitates dissociation of H_2O on an O vacancy of the ceria support.[21] DFT calculations suggest that the reaction of water dissociation takes place at the interface between the Au cluster and the ceria surface with an oxygen vacancy nearby.[14] Recently, Bruix et al. reported the enhanced ability of Pt deposited on stoichiometric CeO_2 (111), that is, on a fully oxidized catalyst, to dissociate O−H bonds of water, suggesting that this step controls the catalytic activity in the WGS reaction.[22]

In this work, we report the investigation of the relationship between catalytic activity toward WGS reaction and the reactivity of vacancies in the support to activate water on well characterized platinum catalysts supported on ceria and ceria doped with gallium. To this aim, we employed a combination of in situ and operando spectroscopic techniques and DFT calculation.

2. EXPERIMENTAL SECTION

2.1. Catalysts. Platinum (1 wt %) catalysts were prepared by an incipient wetness impregnation method from an aqueous solution of $PtNH_4(NO_3)_3$ (Sigma-Aldrich 99.995%) on pure CeO_2 and gallium-doped ceria, $Ce_{0.80}Ga_{0.20}O_{1.90}$ (Ce80Ga20). Supports were synthesized and thoroughly characterized as previously reported.[23−26] The reduction of the catalysts and supports was investigated by temperature-programed reduction with hydrogen, and the metal dispersion was determined by high-resolution TEM (HRTEM) and high-angle annular dark field scanning transmission electron microscopy (HAADF-STEM).

2.2. Catalytic Performance. The catalytic activity of the catalysts for the water gas shift reaction was measured in a fixed-bed stainless steel tubular reactor with inner glass walls (i.d. = 4 mm). A 50 mg portion of catalyst was diluted with 100 mg of quartz and activated in situ by heating from RT to 673 K (10 K min^{-1}) under flowing 5% H_2/He (50 cm^3 min^{-1}), keeping 30 min at this last temperature, then switching to pure He (50 cm^3 min^{-1}, 30 min) and cooling to 373 K. The reaction mixture composition was 1% CO and 2% H_2O balanced with He (total flow = 100 cm^3 min^{-1}). The effluent gas composition was monitored with a calibrated Baltzers QMG 421 quadrupole mass spectrometer.

2.3. Time-Resolved X-ray Diffraction. In situ time-resolved X-ray diffraction (TR-XRD) experiments were carried out on the beamline X7B (λ = 0.3196 Å) of the National Synchrotron Light Source (NSLS) at Brookhaven National Laboratory. The sample was loaded into a heated quartz capillary cell (i.d. = 1 mm) which was attached to a flow system. Two dimensional powder patterns were collected with a Mar345 image plate detector, and the powder rings were integrated using the FIT2D code. Lattice constants were determined by a Rietveld analysis with the program GSAS[27] using LaB_6 as a reference. Diffraction patterns were collected over the catalysts during the WGS reaction and during the isothermal water oxidation experiments. The gases at the outlet of the cell were monitored by mass spectroscopy (SRS rare gas analyzer).

2.4. Isothermal Oxidation by Water. The oxidation by water at 523 K of the Pt reduced catalysts was measured by mass spectroscopy (MS) and in situ diffuse reflectance FTIR (DRIFT). The catalysts were reduced under pure H_2 flow at 523 K for 60 min, followed by purging with Ar for 15 min. Afterward, the samples were oxidized under a flow of 2% H_2O/He. The flow rate was 100 cm^3 min^{-1} in all cases.

The DRIFT measurements were carried out in a high-temperature Harrick cell with ZnSe windows, mounted in a Nicolet 8700 FTIR spectrometer operated with an MCT detector. IR spectra were taken consecutively with an average of 25 scans (acquisition time = 5 s) and a resolution of 4 cm^{-1}. In addition, the oxidation of the reduced samples under flow of 5% O_2/He was also studied at 523 K.

2.5. DFT Calculations. The VASP package v.5.2.12_gamma was used to carry out all the calculations with the Perdew−Burke−Ernzernhof PBE functional.[28−30] The core electrons are kept frozen and replaced by pseudopotentials generated by the plane augmented wave method PAW (O_s, Ce, Pt, Ga_d). The valence electrons (Ce, $5s^2$ $5p^6$ $4f^1$ $5d^1$ $6s^2$; O, $2s^2$ $2p^4$; Ga, $3d^{10}$ $4s^2$ $4p^1$) are explicitly described by means of a plane-wave basis set with a cutoff of 300 eV. The gamma point was used for sampling the Brillouin space. Spin-polarized calculations have been performed for all the systems. The Hubbard parameter, $U - J = 5$, has been included for the Ce 4f levels. The unit cells are displayed and described in more detail in the Supporting Information.

2.6. Concentration-Modulation Excitation Spectroscopy (c-MES). C-MES experiments were performed by periodically switching between two different gaseous atmospheres into the DRIFT cell described above: He and the reaction mixture (1% CO + 2% H_2O) with a frequency (ω) of 4.2 mHz (or 4 min period) at 523 K. Time-resolved spectra were further analyzed using the phase-sensitive detection (PSD) method. More details on the technique and experimental setup can be found in reference 31.

3. RESULTS

3.1. Characterization of the Catalysts and Water Gas Shift Activity Test. Table 1 summarizes the main features of the catalysts. Ceria and ceria−gallia oxides were thoroughly characterized in previous reports,[23−26] and further information is presented in the Supporting Information (SI). It was shown that Ga^{3+} cations incorporate into the ceria lattice producing an actual solid solution.[23,25] The redox properties of these materials have been investigated quantitatively by total or ultimate oxygen storage capacity[26] and temperature-programmed reduction with hydrogen (SI Figure S1). A remarkable increase in the reducibility in the Ga-doped ceria as compared with pure ceria was shown. Moreover, in situ X-ray absorption spectroscopy proved that only Ce^{4+} is reduced to Ce^{3+} and that bulk Ga^{3+} species remain fully oxidized when reducing with hydrogen up to 673 K.[26]

Table 1. Chemical Analysis and Metal Dispersion of Investigated Catalysts

catalyst	Pt[a] (wt %)	Ce/Ga ratio (at %/at %)	Ga[a] (wt %)	D[b] (%)	S_{BET} (m^2/g)
Pt/CeO_2	0.70	100/0	0	90[c]	66
				90[d]	
Pt/Ce80Ga20	0.71	80/20	9.29	92[c]	100
				91[d]	

[a]As determined by inductively coupled plasma (ICP). [b]Metal dispersion measured by TEM (see Supporting Information). [c]activated sample (reduced at 673 K). [d]post-WGS reaction.

dx.doi.org/10.1021/cs500323u | ACS Catal. 2014, 4, 2088−2096

Likewise, platinum-supported catalysts showed the same reducibility trend. Figure 1A,B presents the evolution of the

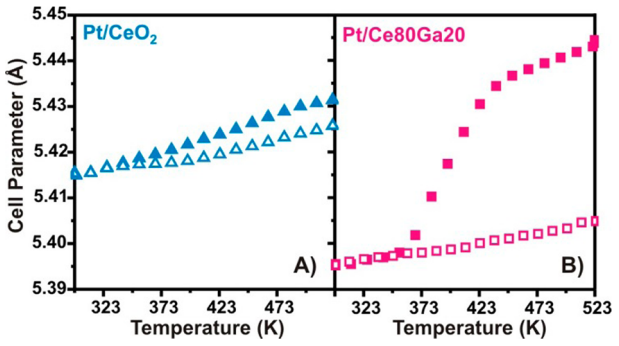

Figure 1. Thermal evolution of the lattice parameter measured by TR-XRD on Pt/CeO_2 (A) and Pt/Ce80Ga20 (B) during the H_2-TPR experiment (solid symbols) and under 5% O_2/He (open symbols).

lattice parameter of each catalyst determined from the (111) diffraction peak obtained by time-resolved X-ray diffraction during the temperature-programed reduction under flowing hydrogen. The open symbols represent the thermal expansion of the lattice parameter under flowing 5%O_2/He, and the solid symbols represent the lattice expansion during H_2-TPR. The initial value of the lattice parameter is slightly lower in the gallium-doped catalyst because of the incorporation of Ga^{3+} cation into the ceria.[23] An increase in the lattice parameter, higher than that expected from the thermal expansion for CeO_2 of about 0.01 Å (e.g., thermal expansion coefficient for ceria in air is $0.86-1.1 \times 10^{-5}$ Å K^{-1} [32−34]) is related to the reduction of ceria because the Ce^{3+} cation is bigger than Ce^{4+}. Then, changes in the ceria lattice parameter can be directly related to the concentration of oxygen vacancies and Ce^{3+} cations in each oxide.[35] For Pt/CeO_2, the increase in the lattice parameter at 523 K under H_2 was 2-fold higher than the one attributed to the thermal expansion (0.023 vs 0.011 Å, Figure 1A, solid symbols vs open symbols), whereas in the case of Pt/Ce80Ga20, the expansion was 5-fold higher (0.05 vs 0.011 Å, Figure 1B, solid symbols vs open symbols), indicating the higher reducibility of the last catalyst.

Platinum metal dispersion of the activated and post-WGS reaction samples was determined by STEM in HAADF mode (SI Figures S2, S3). In all cases, the distributions are particularly narrow, with a mean metal particle diameter of ∼0.8 nm and a metal dispersion of 90%. After reaction, the high metal dispersion remained unchanged on either Pt/CeO_2 or Pt/Ce80Ga20. This last observation, that is, stable Pt dispersion, allows us to compare the reduction and reoxidation by water on this set of catalysts without the extra factor of a changing metal particle size, which is well known to affect the overall rate of those processes.

Figure 2 shows the catalytic activity of the investigated catalysts toward the WGS reaction between 373 and 673 K. Platinum supported on pure ceria presented an onset of the CO conversion at 473 K, with a 50 percent of conversion (T_{50}) at ∼528 K. On the other hand, the platinum catalyst supported on gallium-doped ceria exhibited a lower activity than Pt/CeO_2, with a T_{50} at ∼558 K. The specific reaction rate (X_{CO} < 10%) obtained for the Pt/CeO_2 and Pt/Ce80Ga20 catalysts at 473 K was found to be 1.4 and 0.3 μmol g^{-1} s^{-1}, respectively. It is worth mentioning that the WGS reaction was previously investigated over Au/CeO_2 and Au/Ce80Ga20 catalysts

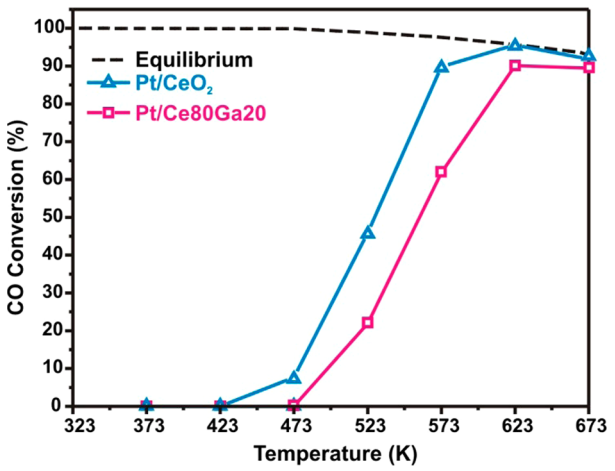

Figure 2. CO conversion at increasing temperature for the WGS reaction. Catalysts: Pt/CeO_2 (triangle) and Pt/Ce80Ga20 (square). Reaction conditions: 1% CO + 2% H_2O balanced with He (total flow = 100 m^3 min^{-1}), 50 mg of catalyst. Dotted line indicates the CO thermodynamic equilibrium conversion.

pretreated under oxidizing conditions (5% O_2/He, 523 K, 1 h; He, 523 K, 1 h).[25] In this case, we were able to study the WGS reaction over catalysts with oxidized ceria and ceria−gallia supports while gold remained in the metallic state. The catalytic activity toward the WGS reaction over Au/CeO_2 and Au/Ce80Ga20 catalysts followed the same trend as the corresponding reduced Pt catalysts shown above.

To investigate the catalysts' redox states, the lattice parameter of the supports was also monitored by time-resolved X-ray diffraction under the WGS reaction at different temperatures. Only the diffraction lines for ceria were observed, indicating that most of the platinum is highly dispersed, as already shown by TEM, and no segregation of Ga_2O_3 has been detected under reaction. Figure 3A,B shows the evolution of the lattice parameters for each supported catalyst determined from (111) diffraction peaks under WGS reaction and the MS traces of CO and CO_2 in the gas phase.

To analyze the redox state of the catalysts during the reaction, it should be noted that platinum catalysts were pretreated in situ in hydrogen to 523 K. Therefore, when exposed to the reaction mixture, the catalysts are already reduced. Consequently, the cell parameter expansion includes the effect of heating and the partial reduction of Ce^{4+} to Ce^{3+}. The values of the lattice parameter expansion after pretreatment under H_2 and after the WGS reaction are summarized in SI Table S1. In the case of Pt/CeO_2, the lattice parameter expansion under the WGS reaction at 523 K was practically identical to that obtained during pretreatment under hydrogen flow at the same temperature (Figure 3A vs Figure 1A). This suggests that the support is partially reduced under WGS reaction conditions and that the degree of reduction under those conditions was similar to that obtained by reduction with H_2 at the same temperature; however, the lattice parameter expansion for Pt/Ce80Ga20 catalyst during the WGS reaction was lower than the expansion measured during pretreatment (0.033 vs 0.04 Å; see Figure 3B vs Figure 1B), thus indicating that although the support is partially reduced under reaction, even to a higher level than Pt/CeO_2, the degree of reduction was lower than that obtained after reduction with hydrogen. It can be concluded that from a bulk point of view, Pt catalysts are partially reduced under WGS reaction and that the gallium-

dx.doi.org/10.1021/cs500323u | ACS Catal. 2014, 4, 2088−2096

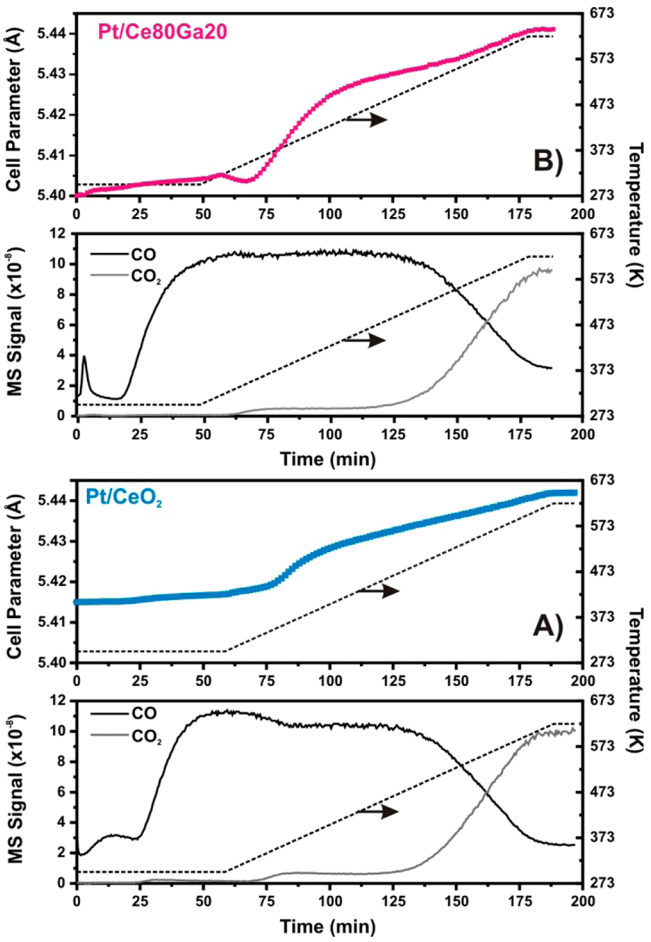

Figure 3. Evolution of the cell parameter and the MS signals for CO and CO_2 as a function of reaction time (WGS) for (A) Pt/CeO_2 and (B) Pt/Ce80Ga20. The dotted line represents the heating ramp. Conditions: 5 mg of catalyst, 1% CO + 2% H_2O, 10 cm^3 min^{-1}.

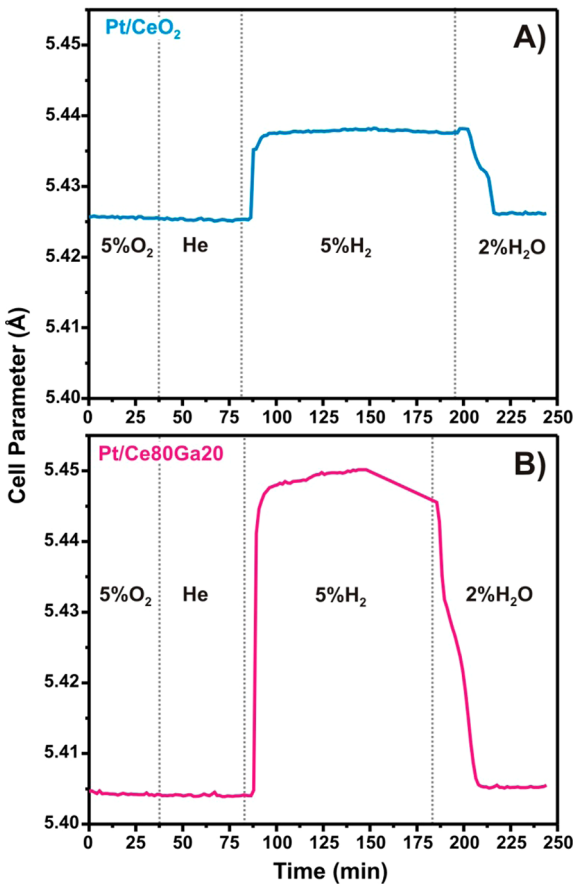

Figure 4. Evolution of the cell parameter during the isothermal oxidation experiments by H_2O at 523 K for reduced catalysts: (A) Pt/CeO_2 and (B) Pt/Ce80Ga20.

doped catalyst showed a higher reduction state, which is somewhat lower than for pure reducing conditions. The bottom panels of Figure 3A,B also show that the onset of the WGS activity, as seen by the evolution of the CO and CO_2 traces, is in agreement with a further expansion of the lattice parameter.

3.2. In Situ Investigation of the Reaction of Ceria Vacancies with Water. To investigate the steps of water activation within the context of the WGS mechanism, a series of experiments were carried out by in situ techniques. The catalysts were reduced, and next, oxidation by exposing the catalysts to a water stream was followed by XRD, DRIFT, and MS. This oxidation process was studied isothermally at 523 K, that is, the temperature at which Pt/CeO_2 and Pt/Ce80Ga20 catalysts showed the highest percentage difference of the WGS activity (see Figure 2).

Figure 4 presents the isothermal (523 K) evolution of the lattice parameter, followed by TR-XRD during a series of reduction−oxidation steps. Notice that no thermal expansion is expected because the temperature was constant along those experiments. After exposing the samples to hydrogen at 523 K, the lattice parameter increased 0.013 and 0.045 Å for Pt/CeO_2 and Pt/Ce80Ga20, respectively, once again confirming the higher reducibility of the mixed oxide support (Figure 4A,B, respectively). After reduction, the catalyst was exposed to a flow of 2% H_2O/He. Thus, the lattice parameter decreased in less than 20 min after exposing the catalysts to steam, indicating that both samples reached an oxidation level similar to the one reached after oxygen treatment. All these results suggest that there is no difference between the bulk oxidation by water of both catalysts.

An additional experiment of oxidation with water at 523 K was performed on the Pt/Ce80Ga20 catalyst but using CO as reducing agent (SI Figure S4). Reduction with 5% CO/He led to an increase in the lattice parameter similar to that obtained under hydrogen (0.041 versus 0.046 Å, respectively), and again, after exposure to water, the support was oxidized to a level similar to that obtained under oxygen.

The isothermal oxidation of the catalyst by water was also investigated by following the concentration of gases at the exit of a plug−flow microreactor by mass spectrometry. Figure 5 shows the evolution of released H_2 ($m/e = 2$) after exposing the reduced catalyst to 2% H_2O/He flow at 523 K. The H_2 released from the Pt/CeO_2 and Pt/Ce80Ga20 was estimated to be 131 and 314 μmol g^{-1}, respectively, that is, in line with the higher reduction of the mixed support. Blank experiments were performed using the bare supports, CeO_2 and Ce80Ga20, but no evolution of H_2 at this temperature was registered. This points out the need for the metal particles to perform this reaction step, as was reported on Au−CeO_2 and Cu−CeO_2.[21]

In addition, the evolution of oxygen vacancies was also investigated by in situ DRIFT spectroscopy following the changes of the Ce^{3+} concentration by means of the forbidden $^2F_{5/2} \rightarrow {}^2F_{7/2}$ electronic transition band at 2130 cm^{-1}.[36] This signal provides very sensitive information from vacancies at the

dx.doi.org/10.1021/cs500323u | ACS Catal. 2014, 4, 2088−2096

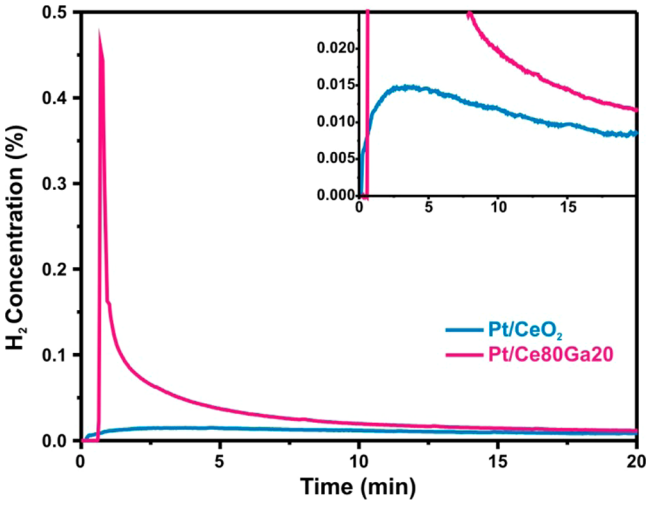

Figure 5. Evolution of H_2 concentration during the isothermal oxidation by H_2O at 523 K.

surface (or subsurface) of the ceria-based materials.[26,37] Figure 6 shows the evolution in the integrated intensity of that band

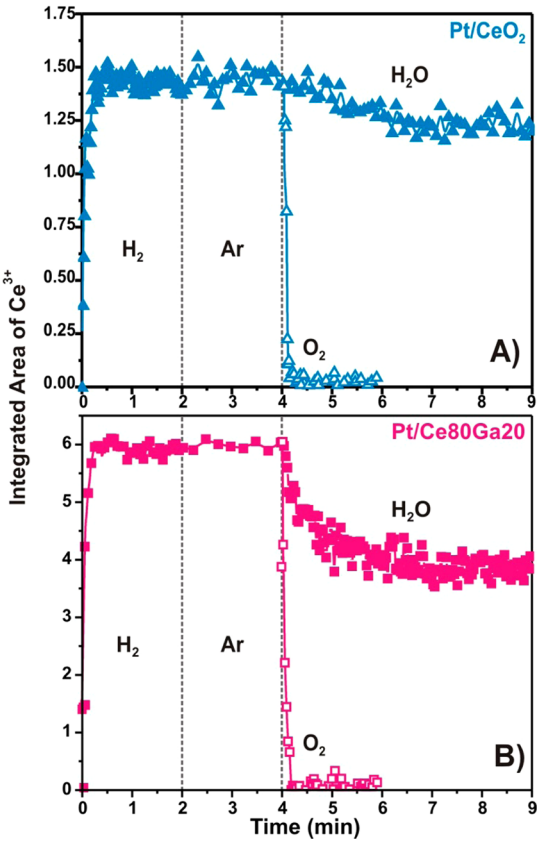

Figure 6. Isothermal evolution of the Ce^{3+} IR signal during the reduction and oxidation by H_2 and water or O_2, respectively, at 523 K for (A) Pt/CeO_2 and (B) PtCe80Ga20.

after the sequential exposure to H_2, Ar, and 2% H_2O/He at 523 K for Pt/CeO_2 and Pt/Ce80Ga20 catalysts. Upon exposure of the oxidized samples to hydrogen, the intensity of the signal at 2130 cm^{-1} increased fast, reaching a plateau after ~15 s (the exchanging time of the DRIFT cell at this flow rate is ~10 s). Again, a higher level of reduction (Ce^{3+} signal intensity) is observed on Pt/Ce80Ga20 than on Pt/CeO_2. Next, the cell was purged with Ar, and sequentially, water was introduced into the cell. The evolution of the Ce^{3+} signal during the oxidation by H_2O presented a progressive decrease until a steady state was achieve at ~120 s. The percentages of oxidation were 23 and 40% for Pt/CeO_2 and Pt/Ce80Ga20, respectively; that is, oxidation was deeper in the case of the mixed oxide. Moreover, the initial rate of the oxidation by water, measured from the slope of the Ce^{3+} signal at 0 min of water admission into the DRIFT cell and normalized by the initial amount of Ce^{3+}, was ~4-fold higher on Pt/Ce80Ga20 than on Pt/CeO_2, which clearly implies a faster oxygen vacancy quenching by water on the first catalyst.

In the same figure, open triangles show the evolution of the Ce^{3+} signal in a similar experiment, but after switching to 5% O_2/He flow instead of water. Note that in these cases, the intensity of the Ce^{3+} band dropped to zero; that is, a complete oxidation after 15 s of exposure to oxygen at 523 K in both Pt/CeO_2 and Pt/Ce80Ga20 catalysts occurred.

3.3. DFT Study of the Oxygen Vacancy Replenishment by Water. The model slabs used for this study are displayed and described in more detail in the Supporting Information (Figure S5). As was shown before, under the WGS reaction, the investigated catalysts present a high degree of reduction. The extent of vacancies and their reaction with water investigated by atomistic thermodynamics allows comparison of the energetics of the two catalysts for different oxygen vacancy contents, then the most favorable compositions for the same external conditions may be determined. Considering the reaction of formation of an oxygen vacancy (eq 1), the Gibbs free energy can be expressed by the working eq 2:

$$MO_x = MO_{x-N} + 1/2NO_2 \quad (1)$$

$$\Delta G = E(MO_{x-N}) + (1/2)NE(O_2) - E(MO_x) + N\Delta\mu(O) \quad (2)$$

where $E(MO_{x-N})$, $E(MO_x)$, and $E(O_2)$ are the computed DFT energies for the reduced and stoichiometric slabs and gas-phase O_2 molecule respectively, N is the number of vacancies, and $\Delta\mu(O)$ is the chemical potential of oxygen with respect to O_2. To account for a wide range of surface reduction, we have computed the energy of the slabs containing 1−8 surface oxygen vacancies for the Pt/CeO_2 and Pt/CeGa models.

The oxygen vacancy formation energies for all the systems calculated are shown in SI Figure S6. The plot of ΔG vs $\Delta\mu(O)$ gives straight lines with slope N for every composition. For a given chemical potential, $\Delta\mu(O)$, the most stable system corresponds to the line with the most negative ΔG value. Figure 7 shows the ΔG-vs-$\Delta\mu(O)$ diagram corresponding to the selected representative systems for Pt/CeO_2 and Pt/CeGa; the diagrams obtained for all the compositions are displayed in SI Figure S6. It can be observed that for oxygen-rich conditions ($\Delta\mu(O)$ close to 0), the stoichiometric slabs are predominant. Decreasing the oxygen chemical potential stabilizes defective slabs: Pt/CeO_2 with one oxygen vacancy is stable for $\Delta\mu(O) < -1.7$ eV, Pt/CeGa with three oxygen vacancies is stable for $\Delta\mu(O) < -1.4$ eV. These slabs are, indeed, the most stable ones for a wide range of chemical potentials (see SI Figure S6). The fact that the Pt/CeGa curves for all values of $\Delta\mu(O)$ lie below the Pt/CeO_2 ones indicates that the Pt/CeGa system is more reducible than Pt/CeO_2. This is confirmed by the analysis of the oxygen vacancy formation energy computed for the

dx.doi.org/10.1021/cs500323u | ACS Catal. 2014, 4, 2088−2096

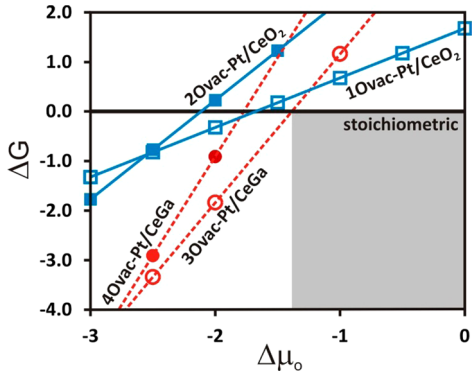

Figure 7. ΔG for reaction 1 as a function of the chemical potential of oxygen $\Delta\mu_O$, in eV. The solid lines are for Pt/CeO_2 models, dashed lines for Pt/CeGa.

defective systems and described in detail in the Supporting Information. The DFT results show then that under the same oxygen chemical potential, the Pt/CeGa system will exhibit 2–3 times more oxygen vacancies than $Pt-CeO_2$. This information is crucial to construct a model for the study of the filling mechanism by water.

The water-filling mechanism step is modeled through the following reaction:

$$MO_x + H_2O = MO_{x+1} + H_2 \quad (3)$$

As stated above, the choice of an appropriate model is crucial to represent realistic conditions. On the basis of the analysis of Figure 7, our starting point will be the one-vacancy Pt/CeO_2 (denoted as $1Ovac/Pt/CeO_2$) and the 3-vacancies Pt/CeGa (denoted as 3Ovac/Pt/CeGa) due to their stability in a wide range of oxygen chemical potential (see SI Figure S6). Previous works in the literature suggest that Pt–O–Ce sites might be the origin of the reactivity in Pt/CeO_2 catalysts.[22]

To model the water-filling of such sites, we have removed a Pt–O–Ce site on each model, thus obtaining the following $MO_x - MO_{x+1}$ model slabs: $2Ovac-1Ovac/Pt/CeO_2$ and 4Ovac–3Ovac/Pt/CeGa. Then the reaction 3 was split into several steps (see Scheme 1 below): I is the reference state (the

Scheme 1. Steps for a Vacancy Refilling with a Water Molecule

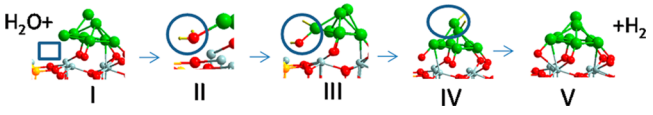

most reduced slab MO_x + a water molecule in the gas phase), II is the molecular adsorption of water in the vacancy, III is the dissociation as OH + PtH, IV is the Pt–HH intermediate after diffusion of H onto the Pt_8 cluster (the oxygen stays in the Pt–O–Ce vacancy position), and V is the final state (oxygen occupying the vacancy in the MO_{x+1} slab, H_2 in the gas phase). In this study, only the intermediates were calculated. Previous calculations on a similar system, that is, water dissociation on a stoichiometric Pt_8/CeO_2 slab model[22] show that the more stable the intermediate, the more stable the associated transition state. On the basis of these results, we focus our analysis on the stability of the reaction intermediates described above.

The relative energies for the intermediates are reported in Table 2. For the 4Ovac–Pt/CeGa system, the reaction is

Table 2. Relative Energy in eV for the Intermediates of the Water-Refilling Mechanism over a Pt–O–Ce Oxygen Vacancy[a]

	I	II	III	IV	V
Pt/CeGa 4Ovac → 3Ovac	0.00	−1.32	−1.10	−2.05	−0.39
Pt/CeO_2 2Ovac → 1Ovac	0.00	−0.90	−1.18	−1.37	−0.13

[a]The intermediates are labeled as in Scheme 1.

exothermic by −0.39 eV. Water adsorbs molecularly; is stabilized by −1.32 eV; then dissociates slightly, destabilizing the system by 0.22 eV; and forms the Pt–HH intermediate, stable by −2.05 eV. The $2Ovac-Pt/CeO_2$ system shows an overall exothermic reaction profile (−0.13 eV). The water intermediate II is stable by −0.90 eV. After dissociation, it stabilizes by −1.18 eV. The Pt–HH intermediate IV is stable by −1.37 eV.

3.4. c-MES DRIFT Investigation of the WGS Reaction.

Isothermal c-MES experiments in combination with PSD analysis were used to monitor the evolution of the surface intermediates using operando DRIFT at 523 K. The MES–PSD methodology is a powerful technique because it allows sensitive and selective spectroscopic detection and monitoring of the dynamic behavior of species directly involved in a reaction.[37,38]

Time-resolved spectra during a complete cycle of ($CO + H_2O$)–He and phase-resolved spectra after applying the PSD algorithm for Pt/CeO_2 and Pt/Ce80Ga20 catalysts are shown in Figure 8. In the 2400–1900 cm^{-1} region of the time domain spectra, the Ce^{3+} band at 2120 cm^{-1} is observed, as expected because of the presence of vacancies under reaction (top panel). However, in the phase-resolved spectra, this signal vanished because it is not affected by the modulation of reactants in both catalysts (bottom panel). Note that small changes in the spectra in that region correspond to the P and R branches of CO(g). These results provide direct evidence of the low participation of the oxygen vacancies under the WGS reaction conditions explored here over platinum supported on ceria-based catalysts.

Conversely, part of the $\upsilon(CO)$ stretching band of CO adsorbed on Pt (peak at 2090 cm^{-1}) and particularly CO_2 in the gas phase (2350 cm^{-1}), are clearly observed to change in the phase-domain spectra. This is due to the change in the conversion of the reaction during the modulation.

More information can be found by analyzing the 3100–2600 and 1800–1100 cm^{-1} spectral regions. In the carbonate region of the time domain spectra, a series of overlapped and broad bands are observed, with a very small variation under modulation. It is worth noting that it is almost impossible to obtain direct information from this spectral region; however, in the phase-resolved spectra, all signals that are from carbonate (1500–1400 cm^{-1}) and bidentate formate (1550, 1370 cm^{-1}) groups vanished, which means that they are spectator species, whereas a minor part can be clearly differentiated. The sharp peaks at 2945, 2830, 2711, 1595, and 1276 cm^{-1} present similar phase delays (320°) and are characteristics of formate species.[39] On the basis of the position and separation between the asymmetric and symmetric OCO stretching modes, $\Delta\nu(COO)$ = 319 cm^{-1}, these signals could be assigned to monodentate formate, m-HCOO:[39−42] $\nu(CH)$ = 2945 cm^{-1} and the

dx.doi.org/10.1021/cs500323u | ACS Catal. 2014, 4, 2088–2096

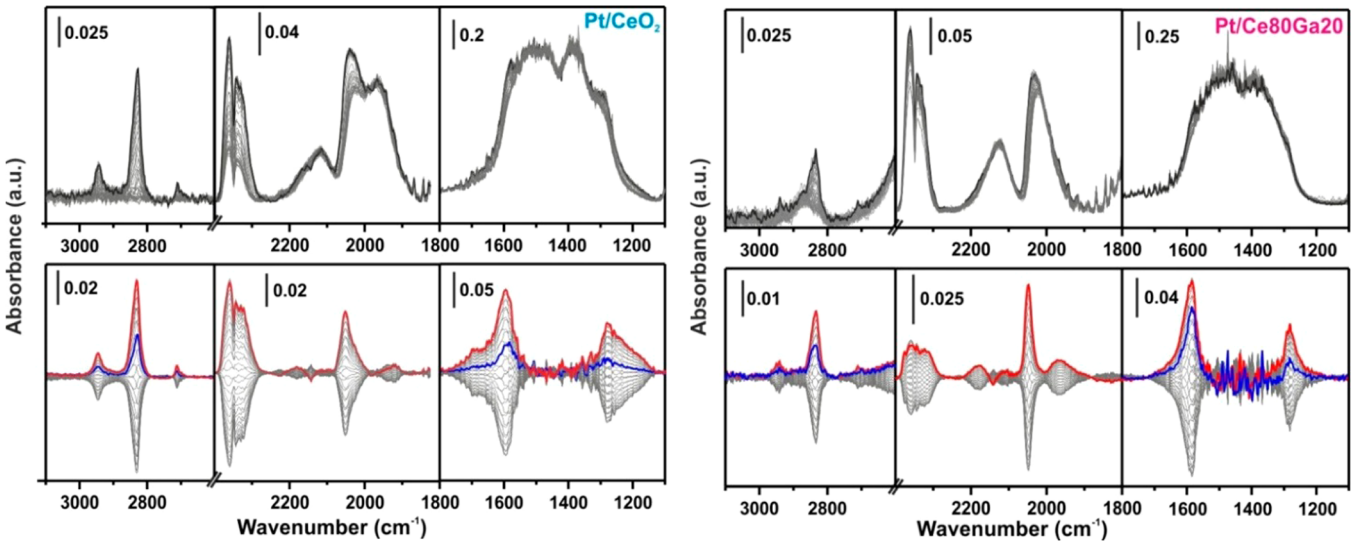

Figure 8. Time domain DRIFT spectra during a c-MES cycle (CO + H_2O)−He (100 cm^3/min, 523 K, ω = 4.2 mHz), over Pt/CeO_2 and Pt/Ce80Ga20 (top panel) and phase domain spectra after PSD demodulation (bottom panel).

combinations $\nu_{as}(OCO) + \delta(CH) = 2830\ cm^{-1}$ and $\nu_s(OCO) + \delta(CH) = 2711\ cm^{-1}$, $\nu_{as}(OCO) = 1595\ cm^{-1}$, $\nu_s(OCO) = 1276\ cm^{-1}$ (see SI Figure S7, Table S2).

In addition, on the Pt/CeO_2 catalyst, two shoulders are observed at 1660 and 1215 cm^{-1} with a phase delay of 330°. Because of the position and splitting of these bands, ∼445 cm^{-1}, they could be ascribed to carboxylate species ($CO_2^{\delta-}$).[43] Recently, evidence of carboxylate species stabilized at the metal−oxide interface on model single crystal $CeO_x/Cu(111)$ and $CeO_x/Au(111)$ catalysts during the WGS reaction has been reported.[21] However, $CO_2^{\delta-}$ has never been detected on powder samples before because of the strong peak intensities of spectator carbonate/formate groups always present in the same spectral region. Thus, on the basis of their surface coordination, the MES−PSD approach allows fingerprint identification of reactive carbonaceous groups that are revealed from the C−O stretching modes during reaction.

4. DISCUSSION

The role and importance of oxygen vacancies to activate a water molecule over highly active low-temperature WGS catalysts based on reducible oxides is a matter of debate. Reports on supported platinum and gold nanoparticles showed a strong dependence of this step on the reducibility of the oxide employed as support. Ribeiro and co-workers[44] showed that the reaction order for water and the apparent activation energy can sharply change when comparing Au/TiO_2 and Au/Al_2O_3 catalysts, concluding that the support directly participates in activating H_2O molecules. Likewise, $Au/CeZrO_2$ and $Pt/CeZrO_2$ catalysts have been investigated by Fonseca et al.[20] They correlated the WGS activity with the more effective H_2O activation of gold than platinum. In addition, it was proposed that the creation of an oxygen vacancy on ceria plays an essential role in water dissociation during the WGS reaction.[19−21] Thus, it was suggested that a higher support reducibility should be correlated with a better catalytic performance in the WGS reaction.

In this work, catalysts based on platinum supported on ceria and ceria−gallia oxides, with similar and stable metal dispersion but with tuned redox properties, were tested in the WGS reaction. The catalytic performance of Pt/CeO_2 was superior to Pt/Ce80Ga20, despite that the gallium-doped support showed a higher capacity to form oxygen vacancies; that is, it is more reducible material. In situ XRD during WGS reaction (1%CO + 1%H_2O) showed that both catalysts are partially reduced during the course of the reaction. Moreover, as stated before, Pt/Ce80Ga20 is more reduced than Pt/CeO_2, indicating that the creation of vacancies is not the rate-limiting step for WGS reaction over these catalysts.

The isothermal oxidation by water at 523 K, a temperature at which Pt/CeO_2 showed a higher WGS activity than Pt/Ce80Ga20, showed that on both catalysts, the vacancies are readily filled (Figure 4 and 5). Following of the signal of Ce^{3+} cations in surface sites by DRIFT spectroscopy (Figure 6) showed a higher but incomplete oxidation in the case of the catalyst doped with Ga compared to pure ceria (40% and 23%, respectively).

The stability of the oxygen vacancies at the metal particle−support interface was investigated by DFT calculations. In agreement with previous reports,[45] results indicate that the doping with gallium stabilized the oxygen vacancy in the surface of the support, as compared with the pure cerium oxide. Concurrently, as experimentally observed, the Pt/CeGa system is more reducible than Pt/CeO_2. The analysis of the Gibbs free energy diagrams in Figure 7 shows that under reductive conditions (poor oxygen chemical potential), the Pt/CeGa slabs contain roughly 2−3 more vacancies than the Pt/CeO_2 ones. This is consistent with the higher reduction observed by XRD in the WGS reaction.

Regarding the mechanism for oxygen vacancies filling by H_2O, the dissociation step of water (intermediate II to III) is slightly endothermic for 4Ovac−Pt/CeGa (0.22 eV) and exothermic for 2Ovac−Pt/CeO_2 (−0.28 eV), although the dissociated intermediates III stabilize in a similar manner for the two materials (−1.10 eV for 4Ovac−Pt/CeGa, −1.18 eV for 2Ovac−Pt/CeO_2). Bruix et al.[22] reported a stabilization of −1.00 eV and −1.24 eV for intermediates II and III in a Pt_8/CeO_2 stoichiometric periodic model, in which water adsorbs and dissociates on top of the Pt_8 particle. Our values, −0.90 and −1.18 eV, respectively, are similar to those obtained in that reference but including the presence of two oxygen vacancies (one below the Pt_8 and one at the Pt−O−Ce site) that take

dx.doi.org/10.1021/cs500323u | ACS Catal. 2014, 4, 2088−2096

into account the effective reduced state of the catalyst after exposure to H_2. The adsorption of water on the Pt−O−Ce vacancy site was found more favorable than the adsorption on the Pt cluster by 0.70 eV. The overall process for the vacancy filling by water was found to be more exothermic in the Pt/CeGa system (−0.39 eV) than for Pt/CeO_2 (∼0.3 eV). This is consistent with the observed higher reoxidation rate for the mixed material.

Altogether, the experimental and DFT results show that the replenishment of vacancies in the support is always fast and the reoxidation by water does not seem to be energetically relevant in ceria-supported catalysts. Moreover, c-MES DRIFT spectroscopy experiments under WGS reaction showed that the Ce^{3+} band at 2120 cm^{-1} is not affected by the perturbation (Figure 8). This last result clearly suggests that although the oxygen vacancies can react with water, as shown before, it is not the rate-determining step in the WGS reaction mechanism on these catalysts.

Thus, all the results discussed above led us to consider that a different type of mechanism operates on these catalysts. The c-MES provided direct evidence that monodentate formate (m-HCOO) and carboxylate ($CO_2^{\delta-}$), probably located at the metal support interface, are reaction intermediates, but carbonate and bidentate formate are mere spectators.

Carboxylate species have been proposed as an indirect probe of the presence of a carboxyl species (HOCO), which are formed by the reaction of adsorbed CO with an OH group at the metal−support interface.[14,17] The carboxyl mechanism for the WGS reaction was theoretically predicted.[14] However, evidence of carboxylate species was found only on single crystals,[17] and here, we report the first observation of this species on powder catalysts.

In addition, monodentate formate can be formed by the isomerization of HOCO species. m-HCOO can decompose to CO_2, but bidentate formates are highly stable and remain in the surface of the support.[46]

C-MES DRIFT results indicated that the Pt/CeO_2 catalyst presented a higher surface coverage of monodente formate and carboxylate species than the Pt/Ce80Ga20, which could explain the higher reactivity observed for the former catalysts. Further experiments are necessary to investigate the role of these intermediates in the WGS mechanism.

5. CONCLUSIONS

Pt/CeO_2 and Pt/Ce80Ga20 catalysts investigated in this work present a remarkable reducibility, enhanced by the incorporation of Ga^{3+} cations, and a very stable metal dispersion. These characteristics allowed the comparison of the formation of oxygen vacancies and the step water activation concerning the water gas shift mechanism on these systems. A series of experimental in situ and operando techniques combined with theoretical calculations allowed us to gain information on the role of the oxygen vacancies in the WGS mechanism. The higher activity found on the Pt/CeO_2 cannot be correlated with the enhanced reducibility and reactivity with H_2O of the Pt/Ce80Ga20. Therefore, the activation of water molecules in the WGS mechanism is not the rate-limiting step in this system. The c-MES results suggest that the low temperature WGS activity exhibited by Pt catalysts could be governed by another step in the "associative mechanism", in which monodente formate (m-HCOO) and carboxylate ($CO_2^{\delta-}$) species at the metal−support interface could be the main reaction intermediates.

■ ASSOCIATED CONTENT

Supporting Information

Details of the unit cells employed during the DFT calculations, characterization of the supports and catalysts (TPR-H_2, metal dispersion by TEM), additional time-resolved XRD results and assignment of the IR bands in the phase-resolved spectra during c-MES experiments. This material is available free of charge via the Internet at http://pubs.acs.org.

■ AUTHOR INFORMATION

Corresponding Author

*E-mail: scollins@santafe-conicet.gov.ar.

Notes

The authors declare no competing financial interest.

[⊥]M. Calatayud has been recognized by the Institut Universitaire de France.

■ ACKNOWLEDGMENTS

This work was supported by the National Council for Scientific and Technical Research (CONICET); the National Agency for the Promotion of Science and Technology (ANPCyT, Grant PICT 2012-1280); and the Universidad Nacional del Litoral (CAID J379) of Argentina (COST CM1104, Eulanest 042, PME 2006 311, CAID 2009 J379, and MINCyT-ECOS A09E01). The work at BNL was financed by the U.S. DOE, Office of BES (DE-AC02-617 98CH10086). M.C. is grateful to HPC GENCI-CINES/IDRIS (Grant 2011-x2011082131) and the CCRE-DSI of Université P. M. Curie for computational resources. B. Diawara is warmly acknowledged for the Modelview visualization program. J.V. thanks the CONICET of Argentina for a grant received to carry out this work.

■ REFERENCES

(1) Zalc, J. M.; Löffler, D. G. *J. Power Sources* **2002**, *111*, 58−64.
(2) Burch, R. *Phys. Chem. Chem. Phys.* **2006**, *8*, 5483−500.
(3) Bunluesin, T.; Gorte, R. J.; Graham, G. W. *Appl. Catal., B* **1998**, *15*, 107−114.
(4) Hilaire, S.; Wang, X.; Luo, T.; Gorte, R.; Wagner, J. *Appl. Catal., A* **2001**, *215*, 271−278.
(5) Ratnasamy, C.; Wagner, J. P. *Catal. Rev.* **2009**, *51*, 325−440.
(6) Kochloefl, K. Water gas shift reaction. In *Handbook of Heterogeneous Catalysis*; Ertl, G., Knozinger, H., Weitkamp, J. Eds.; Wiley-VCH: Weinheim, 1997; Vol. *4*, pp 1831−1840.
(7) Ribeiro, M. C.; Jacobs, G.; Linganiso, L.; Azzam, K. G.; Graham, U. M.; Davis, B. H. *ACS Catal.* **2011**, *1*, 1375−1383.
(8) Shido, T.; Iwasawa, Y. *J. Catal.* **1992**, *136*, 493−503.
(9) Jacobs, G.; Williams, L.; Graham, U.; Sparks, D.; Davis, B. H. *J. Phys. Chem. B* **2003**, *107*, 10398−10404.
(10) Leppelt, R.; Schumacher, B.; Plzak, V.; Kinne, M.; Behm, R. *J. Catal.* **2006**, *244*, 137−152.
(11) Kalamaras, C. M.; Dionysiou, D. D.; Efstathiou, A. M. *ACS Catal.* **2012**, *2*, 2729−2742.
(12) Goguet, A.; Meunier, F. C.; Tibiletti, D.; Breen, J. P.; Burch, R. *J. Phys. Chem. B* **2004**, *108*, 20240−20246.
(13) Meunier, F. C.; Tibiletti, D.; Goguet, A.; Reid, D.; Burch, R. *Appl. Catal., A* **2005**, *289*, 104−112.
(14) Chen, Y.; Wang, H.; Burch, R.; Hardacre, C.; Hu, P. *Faraday Discuss.* **2011**, *152*, 121−133.
(15) Gong, X. Q.; Hu, P.; Raval, R. *J. Chem. Phys.* **2003**, *119*, 6324−6334.
(16) Liu, Z. P.; Jenkins, S. J.; King, D. A. *Phys. Rev. Lett.* **2005**, *94* (196102), 1−4.
(17) Mudiyanselage, K.; Senanayake, S. D.; Feria, L.; Kundu, S.; Baber, A. E.; Graciani, J.; Vidal, A. B.; Agnoli, S.; Evans, J.; Chang, R.;

Axnanda, S.; Liu, Z.; Sanz, J. F.; Liu, P.; Rodriguez, J. A.; Stacchiola, D. J. *Angew. Chem., Int. Ed.* **2013**, *52*, 5101−5105.
(18) Burch, R.; Goguet, A.; Meunier, F. C. *Appl. Catal., A* **2011**, *409*−*410*, 3−12.
(19) Kalamaras, C. M.; Gonzalez, I. D.; Navarro, R. M.; Fierro, J. L. G.; Efstathiou, A. M. *J. Phys. Chem. C* **2011**, *115*, 11595−11610.
(20) Amieiro-Fonseca, A.; Fisher, J. M.; Ozkaya, D.; Shannon, M. D.; Thompsett, D. *Top. Catal.* **2007**, *44*, 223−235.
(21) Rodriguez, J. A.; Liu, P.; Hrbek, J.; Evans, J.; Pérez, M. *Angew. Chem., Int. Ed.* **2007**, *46*, 1329−1332.
(22) Bruix, A.; Rodriguez, J. A.; Ramírez, P. J.; Senanayake, S. D.; Evans, J.; Park, J. B.; Stacchiola, D.; Liu, P.; Hrbek, J.; Illas, F. *J. Am. Chem. Soc.* **2012**, *134*, 8968−8974.
(23) Collins, S.; Finos, G.; Alcántara, R.; Del Rio, E.; Bernal, S.; Bonivardi, A. *Appl. Catal., A* **2010**, *388*, 202−210.
(24) Finos, G.; Collins, S.; Blanco, G.; del Rio, E.; Cíes, J. M.; Bernal, S.; Bonivardi, A. *Catal. Today* **2012**, *180*, 9−18.
(25) Vecchietti, J.; Collins, S.; Delgado, J. J.; Małecka, M.; Rio, E.; Chen, X.; Bernal, S.; Bonivardi, A. *Top. Catal.* **2011**, *54*, 201−209.
(26) Vecchietti, J.; Collins, S.; Xu, W.; Barrio, L.; Stacchiola, D.; Calatayud, M.; Tielens, F.; Delgado, J. J.; Bonivardi, A. *J. Phys. Chem. C* **2013**, *117*, 8822−8831.
(27) Larson, A. C.; von Dreele, R. B. *GSAS General Structure Analysis System; Report LAUR 86-748*; Los Alamos National Laboratory: Los Alamos, NM, 1995.
(28) Kresse, G.; Furthmüller. *J. Phys. Rev. B* **1996**, *54*, 11169−11186.
(29) Kresse, G.; Hafner. *J. Phys. Rev. B* **1993**, *47*, 558−561.
(30) Kresse, G.; Hafner. *J. Phys. Rev. B* **1994**, *49*, 14251−14269.
(31) Aguirre, A.; Collins, S. E. *Catal. Today* **2013**, *205*, 34−40.
(32) Chiang, H. W.; Blumenthal, R. N.; Fournelle, R. A. *Solid State Ionics* **1993**, *66*, 85−95.
(33) Tyagi, A. K.; Ambekar, B. R.; Mathews, M. D. J. *Alloys Compd.* **2002**, *337*, 277−281.
(34) Kossoy, A.; Frenkel, A. I.; Feldman, Y.; Wachtel, E.; Milner, A.; Lubomirsky, I. *Solid State Ionics* **2010**, *181*, 1473−1477.
(35) Barrio, L.; Zhou, G.; González, I. D.; Estrella, M.; Hanson, J.; Rodriguez, J. A; Navarro, R. M.; Fierro, J. L. G. *Phys. Chem. Chem. Phys.* **2012**, *14*, 2192−202.
(36) Binet, C.; Badri, A.; Lavalley, J. C. *J. Phys. Chem.* **1994**, *98*, 6392−6398.
(37) Collins, S. E.; Cies, J. M.; del Rio, E.; Lopez-Haro, M.; Trasobares, S.; Calvino, J. J.; Pintado, J. M.; Bernal, S. *J. Phys. Chem. C* **2007**, *111*, 14371−14379.
(38) Urakawa, A.; Bürgi, T.; Baiker, A. *Chem. Eng. Sci.* **2008**, *63*, 4902−4909.
(39) Busca, G.; Lorenzelli, V. *Mater. Chem.* **1982**, *7*, 89−126.
(40) Li, C.; Domen, K.; Maruya, K. I.; Onishi, T. *J. Catal.* **1990**, *125*, 445−455.
(41) Binet, C.; Daturi, M.; Lavalley, J.-C. *Catal. Today* **1999**, *50*, 207−225.
(42) Collins, S.; Baltanás, M.; Bonivardi, A. *J. Catal.* **2004**, *226*, 410−421.
(43) Gibson, D. H. *Coord. Chem. Rev.* **1999**, *185*−*186*, 335−355.
(44) Shekhar, M.; Wang, J.; Lee, W.; Williams, W. D.; Kim, S. M.; Stach, E. A.; Miller, J. T.; Delgass, W. N.; Ribeiro, F. H. *J. Am. Chem. Soc.* **2012**, *134*, 4700−4708.
(45) Quaino, P.; Syzgantseva, O.; Siffert, L.; Tielens, F.; Minot, C.; Calatayud, M. *Chem. Phys. Lett.* **2012**, *519*−*520*, 69−72.
(46) Calatayud, M.; Collins, S. E.; Baltanás, M. A.; Bonivardi, A. L. *Phys. Chem. Chem. Phys.* **2009**, *11*, 1397−1405.